

Singular value distribution of the propagation matrix in random scattering media

Alexandre Aubry and Arnaud Derode

Institut Langevin, ESPCI ParisTech

CNRS UMR 7587, Université Denis Diderot (Paris VII),

Laboratoire Ondes et Acoustique, 10 rue Vauquelin, 75005 Paris, France

(Dated: February 6, 2020)

Abstract

The distribution of singular values of the propagation operator in a random medium is investigated, in a backscattering configuration. Experiments are carried out with pulsed ultrasonic waves around 3 MHz, using an array of 64 programmable transducers placed in front of a random scattering medium. The impulse responses between each pair of transducers are measured and form the response matrix. The evolution of its singular values with time and frequency is computed by means of a short-time Fourier analysis. The results are compared to the mean distribution of the singular values predicted by random matrix theory. Once the experimental matrix coefficients are renormalized, experimental results and theoretical predictions are found to be in a very good agreement. Two kinds of random media have been investigated: a highly scattering medium in which multiple scattering predominates and a weakly scattering medium. In both cases, residual correlations that may exist between matrix elements are shown to be a key parameter. The mean distribution of singular values exhibits very different behaviours in the single and multiple scattering regimes. The results are applied to the detection of a target embedded in a random scattering medium: a detection criterion is established, based on the statistical properties of the strongest singular value.

PACS numbers: 43.60.+d, 02.10.Yn, 42.25.Dd, 46.65.+g

I. INTRODUCTION

Over the past few years the use of multiple-sensors array in scattering environments has drawn considerable attention, especially in acoustics (array of piezoelectric transducers), electromagnetism (array of antennas) or seismology (array of geophones). Such devices can be used in a transmit configuration, as is the case *e.g.*, in multiple input-multiple output telecommunications for which the spatial diversity brought by the use of multiple-antenna arrays in rich scattering environments allows greater performances [1, 2, 3]. In a backscattering configuration, the array is placed in front of the medium of investigation: it emits an incident wavefield and measures the backscattered signals. This configuration is used for instance in ultrasonic imaging [4], non-destructive testing, sonar and radar [5]. Since array elements can be driven independently both at emission and reception, they are able to shape the emitted/received wavefronts, which offers a variety of applications. All practical applications (communication, detection, imaging, characterization...) and methods (coherent beamforming, intensity measurements, tomography, time-reversal...) despite their diversity, have one thing in common: all the available information is contained in the array response matrix, \mathbf{K} . At each frequency, its coefficients k_{ij} correspond to the complex response between array elements i and j . Once \mathbf{K} is known, the rest is only post-processing. Therefore, in a random scattering environment knowing the statistical properties of \mathbf{K} is essential.

Previous works have been performed in a transmission context, whether it be for communication purposes [6, 7, 8, 9] or scattering problems [10, 11]. In this paper, we will consider backscattering configurations : the same array of N independent elements is used to transmit and receive waves. In that case, \mathbf{K} is a square matrix of dimension $N \times N$, and it is symmetric if the medium is reciprocal. We are particularly interested in the singular value decomposition (SVD) of the propagation operator which amounts to write \mathbf{K} as the product of three matrices: $\mathbf{K} = \mathbf{U}\mathbf{\Lambda}\mathbf{V}^\dagger$. $\mathbf{\Lambda}$ is a diagonal matrix whose nonzero elements λ_i are called the singular values of \mathbf{K} . They are always real and positive, and arranged in a decreasing order ($\lambda_1 > \lambda_2 > \dots > \lambda_N$).

It is now well known that in the case of point-like scatterers in a homogeneous medium, each scatterer is mainly associated to one non-zero singular value of \mathbf{K} [12, 13], as long as the number of scatterers is smaller than N and multiple scattering is neglected [14, 15]. So a singular value decomposition of \mathbf{K} (or equivalently a diagonalisation of the so-

called time-reversal operator $\mathbf{K}\mathbf{K}^*$) allows the selective detection of several targets, each being associated to a singular value of \mathbf{K} . This is the core of a detection method named DORT (French acronym for Decomposition of the Time Reversal Operator) [12, 13]. DORT has shown its efficiency in detecting and separating the responses of several scatterers in homogeneous or weakly heterogeneous media [12, 16] as well as in waveguides [17, 18, 19]. It has found applications in non-destructive evaluation [20], underwater acoustics [21, 22], electromagnetism [23, 24, 25, 26] and in radar applied to forest environments [27, 28, 29].

In this paper we will deal with random scattering media, consisting of a large number ($\gg N$) of randomly distributed scatterers, showing possibly multiple scattering between them. We will also address the issue of detecting a stronger reflector hidden in a statistically homogenous scattering medium, based on the strongest singular value λ_1 . Since the propagation medium is considered as one realisation of a random process, some very general results of random matrix theory (RMT) may be fruitfully applied.

RMT has been widely used in physics, statistics and engineering. The domain of applications are numerous, ranging from nuclear physics [30] or chaotic systems [31] to neural networks [32], telecommunications [6] or financial analysis [33]. RMT predicts general behaviours of stochastic systems as, for instance, determining the Shannon capacity for MIMO communications in random media [8, 9] or statistical properties of highly excited energy levels for heavy nuclei [30]. Another direct application of RMT is to separate the deterministic and random contributions in multivariate data analysis [34, 35, 36].

Here, the experimental configuration we consider uses a piezo-electric array, with a finite ($N = 64$) numbers of elements sending wide-band ultrasonic waves around 3 MHz in an a priori unknown scattering medium. The main issues we address in this work are the applicability of RMT [6] to this experimental context, and its interest to establish a detection criterion based on the statistical properties of λ_1 . Since \mathbf{K} is random, the relevant observable is the probability distribution function $\rho(\lambda)$ of its singular values. Recent experiments [37] indicate that in a multiple scattering regime, the distribution of the singular values is in good agreement with a simple law derived from RMT, the so-called “quarter circle law” $\rho_{QC}(\lambda) = \sqrt{4 - \lambda^2}/\pi$ ($0 < \lambda < 2$) [6, 38]. In theory, the quarter circle law applies to square matrices of infinite dimensions, containing independently and identically distributed elements, with zero-mean and variance $1/N$.

Yet, from a physical point of view some of these assumptions do not hold: in a backscat-

tering configuration the matrix elements are neither independent nor identically distributed, for several reasons (among others, reciprocity and weak localisation). In particular, the field-field correlations that may exist between matrix elements is a key parameter [7, 8, 9, 34]. Moreover when single scattering dominates, the spectral behaviour of \mathbf{K} is shown to be similar to that of a random Hankel matrix (*i.e.*, whose elements are constant along each antidiagonal), and not a “classical” random matrix. This is due to the persistence of a deterministic coherence between single-scattered signals along the antidiagonals of the matrix \mathbf{K} despite randomness, which does not occur in the multiple-scattering regime [37]. Therefore in a practical situation, the probability distribution function $\rho(\lambda)$ may differ significantly from the simple quarter circle law. Finally, in the last part of this paper we consider the detection of a target embedded in a random scattering medium. If a strong target is present, hopefully it should be associated to the strongest singular value λ_1 . We introduce a detection criterion based on the results of the first part. This approach can be generalized to target detection in noisy environments.

II. EXPERIMENTAL PROCEDURE

The experiment takes place in a water tank. We use a N -element ultrasonic array ($N = 64$) with a 3 MHz central frequency and a 2.5-3.5 MHz bandwidth; each array element is 0.39 mm in size and the array pitch p is 0.417 mm. The sampling frequency is 20 MHz. The array is placed in front of the medium of interest. The first step of the experiment consists in measuring the inter-element matrix (see Fig. 1). A 100- μ s-long linear chirp is emitted from transducer i into the scattering sample immersed in water. The backscattered wave is recorded with the N transducers of the same array. The operation is repeated for the N emitting transducers. The response from transducer i to transducer j is correlated with the emitted chirp, which gives the impulse response $h_{ij}(t)$. The $N \times N$ response matrix $\mathbf{H}(t)$ whose elements are the N^2 impulse responses $h_{ij}(t)$ is obtained. Because of reciprocity, $h_{ij}(t) = h_{ji}(t)$ and $\mathbf{H}(t)$ is symmetric. We take as the origin of time ($t = 0$) the instant when the source emits the incident wave.

A scattering medium is essentially characterized by its scattering mean-free path l_e , and its diffusion constant D . If the scattering path length within the medium is larger than l_e , multiple scattering can predominate. This is expected to happen at late times in the

scattered signals $h_{ij}(t)$.

The impulse response matrix $\mathbf{H}(t)$ is truncated into short time windows in order to keep the temporal resolution provided by acoustical measurements and study the transition from a single scattering to a multiple scattering regime. The time signals $h_{ij}(t)$ are truncated into

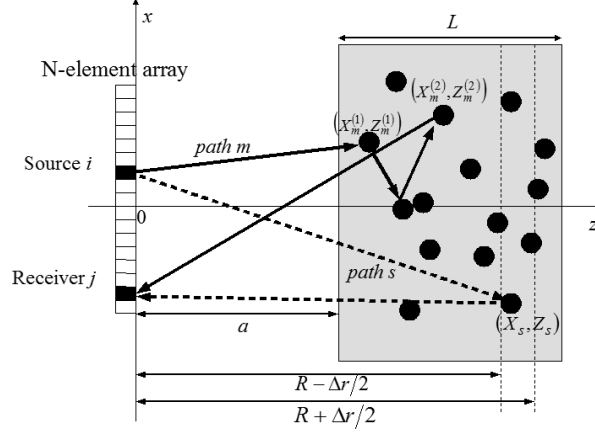


FIG. 1: Experimental setup. A 64-element array is placed in front of a random medium at a distance a . The whole setup is immersed in a water tank. The inter-element response $k_{ij}(T, f)$, around the time of flight T and at the frequency f , is measured. It contains contributions of single and multiple scattering paths whose lengths belong to the interval $[R - \Delta r/2; R + \Delta r/2]$, where $R = cT/2$ and $\Delta r = c\Delta t/2$. Examples of a single scattering path (labelled s , dashed line) and of a multiple-scattering path (labelled m , continuous line) is drawn. (X_s, Z_s) are the coordinates of the scatterer involved in path s . $(X_m^{(1)}, Z_m^{(1)})$ and $(X_m^{(2)}, Z_m^{(2)})$ are the coordinates the first and last scatterers along path m .

overlapping windows : $k_{ij}(T, t) = h_{ij}(T - t)W_R(t)$ with $W_R(t) = 1$ for $t \in [-\Delta t/2, \Delta t/2]$, $W_R(t) = 0$ elsewhere. The value of Δt is chosen so that signals associated with the same scattering path within the medium arrive in the same time window. The detailed calculation of Δt is given in Appendix A. In our experiments, we have typically $\Delta t \sim 30$ periods. At each time T , the k_{ij} form a matrix \mathbf{K} . A short-time Fourier analysis is achieved by a discrete Fourier transform (DFT) and gives the response matrices $\mathbf{K}(T, f)$ at time T and frequency f . The numerical SVD of each matrix \mathbf{K} is performed and yields N singular values $\lambda_i(T, f)$ at each time T and frequency f .

The next step consists in studying the distribution of singular values. It should be noted that we only have access to one realisation of disorder: the scattering medium is fixed, there

is no ensemble averaging. Experimentally, the ensemble average can only be estimated by an average over frequency, and/or an average over time. The universal results provided by RMT are based upon the assumption that the elements of the random matrix have zero mean and a variance of $1/N$. The first condition is easily met, assuming that $k_{ij}(T, f)$ is a superposition of scattering contributions with a phase uniformly distributed between π and $+\pi$. In order to fulfill the second condition and compare experimental and theoretical results, \mathbf{K} is renormalized into $\tilde{\mathbf{K}}$ with normalized singular values $\tilde{\lambda}_i$

$$\tilde{\lambda}_i = \frac{\lambda_i}{\sqrt{\frac{1}{N} \sum_{p=1}^N \lambda_p^2}} \quad (1)$$

Once this renormalization is achieved, the experimental singular values distribution can be investigated. First, we form the histogram $\mathcal{H}(\lambda)$ of the whole set of renormalized singular values $\tilde{\lambda}_i(T, f)$, taken at every rank i , time T and frequency f . Bins of this histogram are the intervals $[mw; (m+1)w]$, where w is the bin width and m is a non-negative integer. $\mathcal{H}(\lambda)$ denotes the number of singular values $\tilde{\lambda}_i(T, f)$ contained in the same bin as λ . An estimator of the probability density function of the singular values is obtained:

$$\hat{\rho}(\lambda) = \frac{\mathcal{H}(\lambda)}{nw} \quad (2)$$

n is the total number of singular values ($n = N \times n_T \times n_f$, n_T is the number of time windows considered and n_f the number of frequencies at which the DFT of k_{ij} is achieved). At early times ($cT - 2a < l_e$) multiple scattering can be neglected, whereas at later times ($cT - 2a \gg l_e$) multiple scattering dominates. In the following of the study, the theoretical singular values distribution predicted by RMT will be confronted to the experimental estimator $\hat{\rho}$, both in multiple and single scattering regimes.

III. MULTIPLE-SCATTERING REGIME

A. Experimental configuration

Here, we study the multiple-scattering regime. To that aim, we use a random-scattering slab consisting of parallel steel rods ($c_L = 5.7 \mu\text{s}$, $c_T = 3 \mu\text{s}$, radius 0.4 mm, density 7.85 kg/L) randomly distributed with a concentration $n=12$ rods/cm². The frequency-averaged elastic mean-free path l_e is 7.7 ± 0.3 mm between 2.5 and 3.5 MHz [39]. The distance a

between the array and the scattering sample is 25 mm. The slab thickness L is 40 mm. Even in such strongly diffusive media, single scattering occurs for small times of flight. Here, we will consider times of flight T larger than $70\mu s$, corresponding to scattering path lengths more than 7 mean free paths. Under these conditions, single scattering can be neglected and $\tilde{\mathbf{K}}$ only contains multiple scattering contributions. The whole experimental procedure described in Sec.II is achieved and a set of renormalized matrices $\tilde{\mathbf{K}}(T, f)$ is obtained. The time-window length Δt is directly deduced from the calculation shown in Appendix A and is set to $10\mu s$.

B. Experimental distribution of singular values

We perform singular value decompositions of $\tilde{\mathbf{K}}(T, f)$ and obtain the estimator $\hat{\rho}(\lambda)$ as defined in Eq.2. According to RMT, if the matrix coefficients \tilde{k}_{ij} are complex random variables independently and identically distributed with zero mean and a variance of $1/N$, then the asymptotic (*i.e* for $N \rightarrow \infty$) density function of its singular values is given by the quarter circle law [6, 38]. As we can see in Fig.2, the experimental distribution of singular

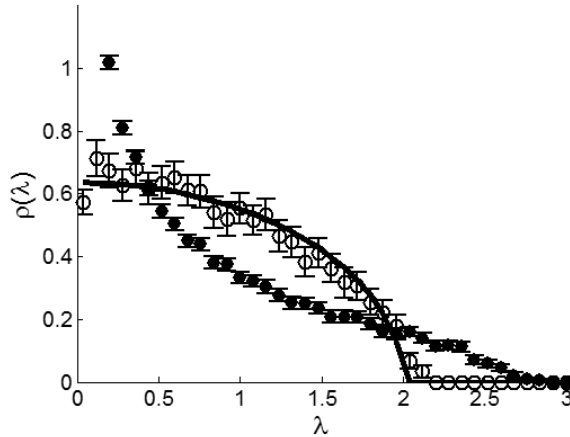


FIG. 2: Experimental distributions of singular values of $\tilde{\mathbf{K}}$ (black disks) and $\tilde{\mathbf{K}}_t$ (white disks) are compared to the quarter circle law (black continuous line). The error bars are \pm two standard deviations.

values is very far from this prediction. The major reason for this discrepancy is that the coefficients \tilde{k}_{ij} are not independent. The experimental matrix $\tilde{\mathbf{K}}$ exhibits strong correlations

between neighbour entries. They are measured by the correlation coefficient Γ_m

$$\Gamma_m = \frac{\langle \tilde{k}_{i,j} \tilde{k}_{i,j+m}^* \rangle_{T,f,(i,j)}}{\langle |\tilde{k}_{i,j}|^2 \rangle_{T,f,(i,j)}} = \frac{\langle \tilde{k}_{i,j} \tilde{k}_{i+m,j}^* \rangle_{T,f,(i,j)}}{\langle |\tilde{k}_{i,j}|^2 \rangle_{T,f,(i,j)}} \quad (3)$$

where the symbol $\langle . \rangle$ denotes an average over the variables in the subscript, *i.e* time T , frequency f and source/receiver pairs (i, j) . The integer $m = i - j$ represents the distance between sources or receivers, in units of p (the array pitch). Fig.3(a) clearly points out a strong correlation between neighbour entries, with a coefficient $\Gamma_1 = \Gamma_{-1} \simeq 0.5$. The physical origin of these correlations will be detailed in Sec.III D. We will also show how to incorporate these correlations into the theoretical model for $\rho(\lambda)$.

In this particular case, correlations can be simply removed by considering only one in two elements. From the initial matrix \mathbf{K} of dimension $N \times N$, a truncated matrix \mathbf{K}_t of dimension $N/2 \times N/2$ is built, considering only elements of odd or even index. \mathbf{K}_t no longer exhibits short range correlations at emission and reception. The experimental distribution of normalized singular values is now much closer to the quarter circle law (see Fig.2). Nevertheless, a slight disagreement remains between the theoretical and experimental curves, specially at the vicinity of $\lambda = 0$ and $\lambda = 2$.

In the next paragraph, we show that in the multiple scattering regime the variance of the matrix entries k_{ij} is not the same for all pairs (i, j) , contrary to the assumption of identically distributed random variables. The consequence of this deviation from RMT assumptions will be discussed.

C. Variance of coefficients \tilde{k}_{ij} .

The signals $k_{ij}(T, f)$ at a time T and frequency f correspond to the sum of partial waves that reach the array in the time window $[T - \Delta t/2; T + \Delta t/2]$. They are associated with multiple scattering paths whose length belongs to the interval $[R - \Delta r/2; R + \Delta r/2]$, with $R = cT/2$ and $\Delta r = c\Delta t/2$ (c is the wave speed in the surrounding medium). An example of such paths is drawn in Fig.1. The response $k_{ij}(T, f)$ can be decomposed into a sum of partial waves associated with the N_q paths. In a 2D configuration, under the paraxial approximation

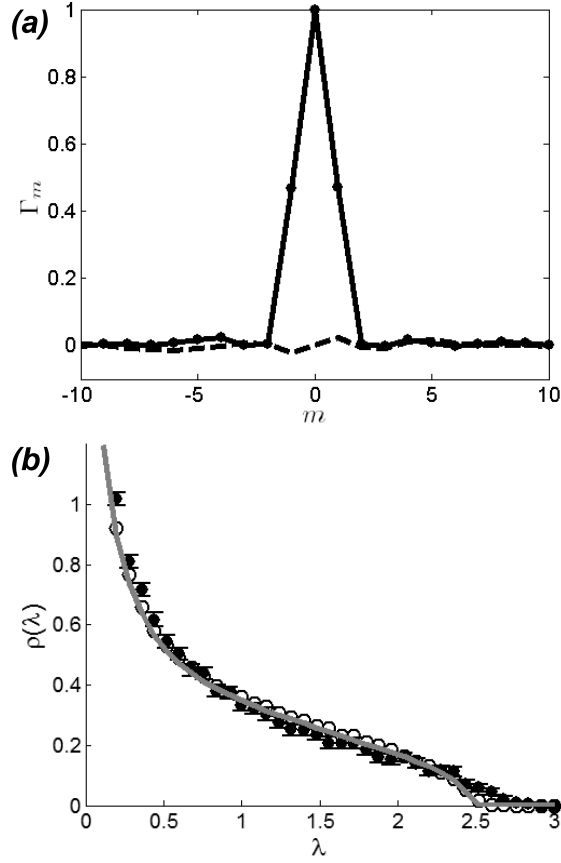


FIG. 3: (a) Normalized correlations Γ_m (real part : continuous line; imaginary part : dashed line) estimated from experimental results. (b) The experimental distribution of singular values (black disks) is compared to the theory taking into account correlations (grey continuous line) and to the result of the numerical simulation (white disks) described in Sec.IIID. The error bars are \pm two standard deviations.

and assuming point-like transducers and scatterers, $k_{ij}(T, f)$ can be expressed as

$$k_{ij}(T, f) \propto \sum_{q=1}^{N_q} B_q \frac{\exp \left[jk \left(Z_q^{(1)} + Z_q^{(2)} \right) \right]}{\sqrt{Z_q^{(1)} Z_q^{(2)}}} \exp \left[jk \frac{\left(x_i - X_q^{(1)} \right)^2}{2Z_q^{(1)}} \right] \exp \left[jk \frac{\left(x_j - X_q^{(2)} \right)^2}{2Z_q^{(2)}} \right] \quad (4)$$

where $k = 2\pi f/c$ is the wave number in the surrounding medium. The index q denotes the q^{th} path which contributes to the signal received at time T . $\left(X_q^{(1)}, Z_q^{(1)} \right)$ and $\left(X_q^{(2)}, Z_q^{(2)} \right)$ are respectively the coordinates of the first and last scatterers along the path q . B_q is the complex amplitude associated with path q , from the first scattering event at $\left(X_q^{(1)}, Z_q^{(1)} \right)$

until the last one at $(X_q^{(2)}, Z_q^{(2)})$. From the central limit theorem, we expect that the coefficients k_{ij} are gaussian complex random variables.

The renormalization (Eq.1) leads to a set of matrices $\tilde{\mathbf{K}}$. If the k_{ij} were identically distributed, the renormalized coefficients \tilde{k}_{ij} would be complex random variables with variance $\sigma_{ij}^2 = 1/N$. Actually, Fig.4(a) shows that σ_{ij}^2 is not uniform over the pairs (i, j) . The

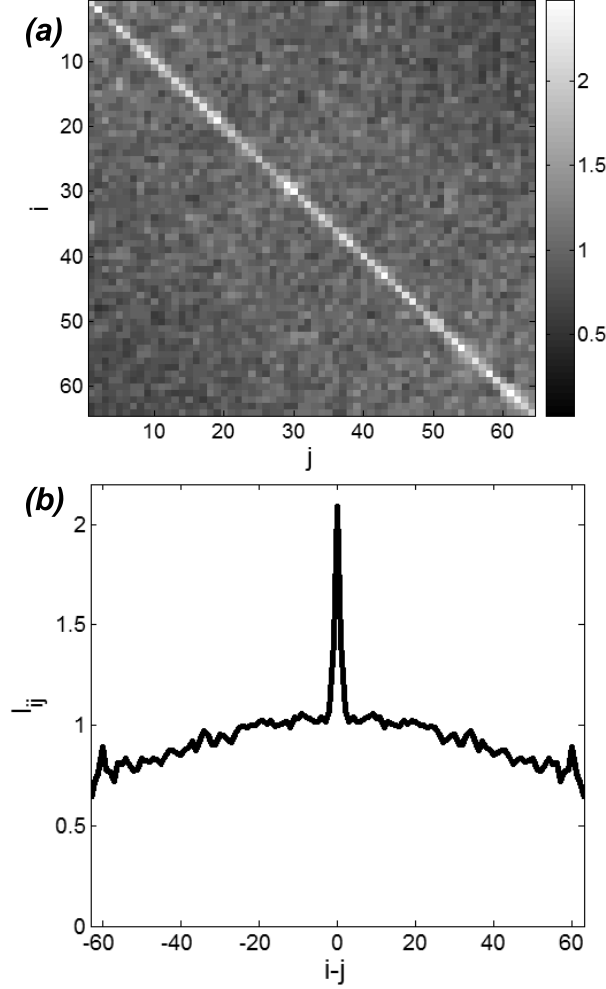


FIG. 4: (a) Mean intensity I_{ij} of coefficients \tilde{k}_{ij} , normalized by $\frac{1}{N}$. Results have been averaged over all times T and frequencies f . (b) I_{ij} as a function of $i - j$ (an average is achieved over couples (i, j) such that $(i - j) = \text{constant}$).

intensity $I_{ij} = \left\langle \left| \tilde{k}_{ij} \right|^2 \right\rangle_{T,f}$ averaged over time T and frequency f is displayed for each source/receiver couple (i, j) . It serves as an estimate of the variance σ_{ij}^2 . The diagonal elements \tilde{k}_{ii} exhibit a double variance compared to the off-diagonal elements. Moreover, the

variance of off-diagonal elements tends to decrease when the distance $|i - j|p$ between the source and the receiver increases. From these results, it appears that the variance of the matrix entries, instead of being the same for all pairs (i, j) , could be modelled as

$$N\sigma_{ij}^2 = N \left\langle \left| \tilde{k}_{ij} \right|^2 \right\rangle \simeq \delta_{ij} + f(|i - j|) \quad (5)$$

where δ is the Kronecker symbol and f a slowly decaying function such that $f(0) = 1$.

The double variance of diagonal elements compared to the off-diagonal ones is well explained by the *coherent backscattering effect* [40, 41, 42]. It corresponds to an enhancement (by a factor of 2) in the intensity of waves scattered in the backward direction. This phenomenon, also known as weak localization, originates from a constructive interference between a wave traveling along a multiple-scattering path and its reciprocal counterpart: it appears when multiple scattering occurs, as long as the reciprocity symmetry is preserved. When source and receiver are identical ($i = j$), any path q whose first and last scatterers are of coordinates $(X_q^{(1)}, Z_q^{(1)})$ and $(X_q^{(2)}, Z_q^{(2)})$, interfere constructively with its reciprocal counterpart whose first and last scatterers are located respectively at $(X_q^{(2)}, Z_q^{(2)})$ and $(X_q^{(1)}, Z_q^{(1)})$. As a consequence, on average, the diagonal elements \tilde{k}_{ii} have a variance twice that of off-diagonal elements. Actually, this effect could also affect the matrix elements close to the diagonal. The typical width of the coherent backscattering peak is $\frac{a}{k\sqrt{D(T-2a/c)}}$ [43, 44], which has to be compared to the array pitch. In this experimental configuration, we have $T > 70 \mu s$, $D \simeq 4 mm^2/\mu s$ [45], $a = 25 mm$ hence $\frac{a}{k\sqrt{D(T-2a/c)}} < 0.16 mm$, whereas the array pitch is $p = 0.417 mm$. Therefore the enhancement due to coherent backscattering is strictly limited to the diagonal elements. Finally, upon renormalization (Eq. 1), taking the coherent backscattering effect into account amounts to rewrite the variance of \tilde{k}_{ij} as $\sigma_{ij}^2 = \frac{1+\delta_{ij}}{N+1}$ (see Appendix B).

Now, one can wonder if the double variance of diagonal elements \tilde{k}_{ii} has any influence on the distribution of the singular values. It is shown in Appendix B that if the matrix dimension N is large enough, the influence of the coherent backscattering peak can be neglected as long as it is limited to the diagonal elements $\left(\frac{a}{k\sqrt{DT}} < p\right)$, provided that the matrix is renormalized according to Eq.1. We will therefore consider that the coherent backscattering enhancement has no significant effect on the distribution of singular values.

The double variance along the diagonal of $\tilde{\mathbf{K}}$ is not the only deviation from the identical distribution assumption. Indeed, if we focus on the dependence of σ_{ij}^2 as a function of $(i - j)$

(see Fig.4(b)), we observe that it is not uniform: it decreases with the distance $x = |i - j|p$ between the source i and the receiver j . This is due to the progressive growth of the diffusive halo (i.e the mean intensity) inside the medium. It is not instantaneous but depends on the diffusion constant D [46]. In a near-field configuration ($a \ll Np$, Np being the array size), σ_{ij}^2 would decrease as $\exp\left(-\frac{x^2}{4DT}\right)$. And as soon as \sqrt{DT} becomes significantly larger than the array size (Np), σ_{ij}^2 can be considered as constant [47]. In a far-field situation ($a \gg Np$), σ_{ij}^2 is always constant, as long as $i \neq j$. The experimental case we study corresponds to an intermediate configuration between near and far field.

A solution to deal with the variations of σ_{ij}^2 is to compensate for them. σ_{ij}^2 depends only on time T and $|i - j|$ (Eq.5). Thus we can estimate σ_{ij}^2 by averaging $\left|\tilde{k}_{ij}(T, f)\right|^2$ over frequency f and elements (i, j) which are separated by the same amount $m = |i - j|$:

$$\hat{\sigma}^2(T, m) = \left\langle \left|\tilde{k}_{ij}(T, f)\right|^2 \right\rangle_{f, \{(i, j) \mid m=|i-j|\}} \quad (6)$$

where $\hat{\sigma}^2(T, m)$ is the estimator of σ_{ij}^2 . Then, at each time T , matrix entries \tilde{k}_{ij} are normalized once again as:

$$\tilde{k}_{ij}^C(T, f) = \frac{\tilde{k}_{ij}(T, f)}{\sqrt{\hat{\sigma}^2(T, |i - j|)}} \quad (7)$$

A set of compensated matrices $\tilde{\mathbf{K}}^C(T, f)$ is built from $\tilde{\mathbf{K}}$. One can show that these matrices satisfy the identical distribution property : the variance of elements \tilde{k}_{ij}^C is now constant over all pairs (i, j) . Once this operation is achieved, the new distribution of singular values can be investigated and is plotted in Fig.5(a). However, the two sets of matrices $\tilde{\mathbf{K}}_t$ and $\tilde{\mathbf{K}}_t^C$ lead to similar singular value spectra. It means that in our case the variations of σ_{ij}^2 with $|i - j|$ are not sufficiently large to significantly modify the distribution of the singular values. Nevertheless, in other experimental configurations, the non-uniformity of σ_{ij}^2 could have a stronger influence. For instance, in a near-field configuration, the growth of the diffusive halo is more visible and the distribution of singular values would exhibit stronger deviations from the quarter circle law, specially at early times.

D. Influence of correlations on the singular spectrum of $\tilde{\mathbf{K}}$

As we can see in Fig.3(a), the experimental matrix $\tilde{\mathbf{K}}(T, f)$ exhibits correlations between adjacent entries. There are two reasons for that. First, there is a mechanical coupling

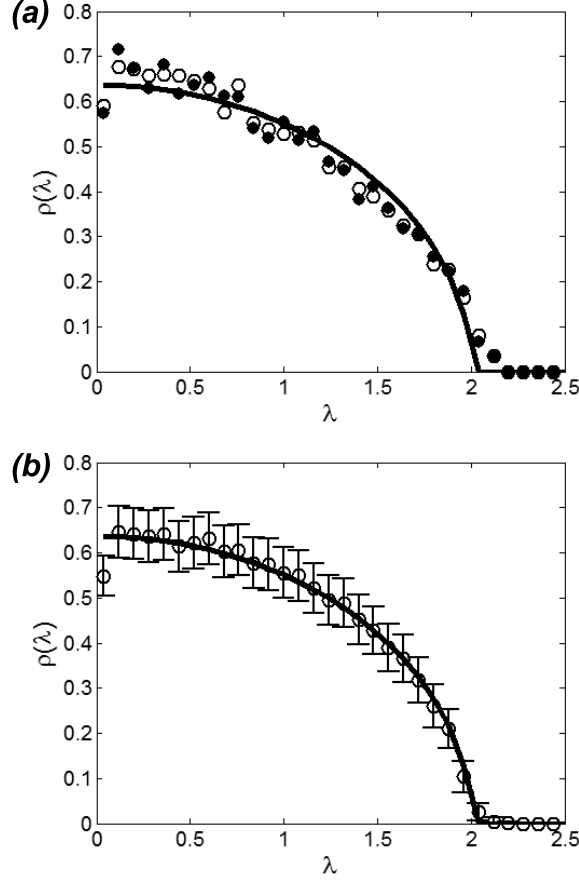


FIG. 5: (a) Influence of the non-uniform variance of k_{ij} : The experimental distributions of singular values for $\tilde{\mathbf{K}}_t$ (black disks) and $\tilde{\mathbf{K}}_t^C$ (white disks) are compared to the quarter circle law (black continuous line). (b) Influence of the symmetry of \mathbf{K} : the result of the numerical simulation (white disks) is compared to the quarter-circle law (black continuous line). The error bars are \pm two standard deviations.

between neighboring array elements. Second, the wave recorded on the array can be seen as the radiation of a spatially incoherent source with width W (the diffuse halo inside the multiple-scattering medium) observed at a distance a . The Van Cittert-Zernike theorem[48, 49] states that the typical coherence length of the wave field is $\lambda a/W$ (in other words, the waves radiated by a finite-size incoherent source see their coherence length increases as they propagate). These two effects result in a short-range correlation between the scattered signals recorded on the array. In the experimental situation we investigated, these residual correlations are limited in range to adjacent elements, both in emission and reception, as it is shown in Fig3(a). They are mainly due here to the mechanical coupling between neighboring

array elements, the coherence length of the diffuse wave-field becoming rapidly smaller than the array pitch in our experimental configuration.

Sengupta and Mitra[34] have investigated theoretically the influence of correlations on the distribution of singular values in the case of large-dimension random matrices. Their model assumes first that $\langle \tilde{k}_{ij} \rangle = 0$. The correlation between two coefficients \tilde{k}_{il} and \tilde{k}_{jm} is expressed as

$$\langle \tilde{k}_{il} \tilde{k}_{jm}^* \rangle = N^{-1} c_{ij} d_{lm} \quad (8)$$

where the symbol $\langle . \rangle$ denotes an ensemble average. \mathbf{C} and \mathbf{D} are $N \times N$ matrices. We will refer to them as the correlation matrices. Based on Eq.8, Sengupta and Mitra predict the distribution of singular values using diagrammatic and saddle point integration techniques. Only the eigenvalues of \mathbf{C} and \mathbf{D} are required to obtain the singular values distribution of \mathbf{K} .

We now apply the Sengupta and Mitra's approach to our experimental configuration. Here, the coefficients c_{ij} and d_{ij} are identical because of spatial reciprocity : $\mathbf{C} \equiv \mathbf{D}$. We estimate c_{ij} by the correlation coefficient Γ_{i-j} defined in Eq.3 :

$$\hat{c}_{ij} = \Gamma_{i-j} \quad (9)$$

The coefficients \hat{c}_{ij} form a matrix $\hat{\mathbf{C}}$ which is an estimator of the correlation matrix \mathbf{C} . $\hat{\mathbf{C}}$ is a Toeplitz matrix : its coefficients only depend on $i - j$. The application of Sengupta and Mitra's approach to our experimental situation embodies two assumptions :

- The correlation between two signals received(emitted) by the same element l and emitted(received) by two elements i and j does not depend on the element l but only on the distance $|i - j|$.
- The correlation between two signals emitted and received by two pairs of elements (i, l) and (j, m) is given by the product of correlations at emission (Γ_{i-j}) and at reception (Γ_{l-m}).

The first assumption requires the random medium to be statistically invariant by translation. The second one is made for analytical tractability and is verified in our case.

Once the correlation coefficient Γ_m is measured experimentally at emission/reception (see Fig.3(a)), the correlation matrix \mathbf{C} is estimated by $\hat{\mathbf{C}}$ (Eq.9). Eigenvalues of $\hat{\mathbf{C}}$ are

calculated numerically and incorporated in Sengupta and Mitra's model in order to obtain an estimation of the singular value distribution for $\tilde{\mathbf{K}}$.

In Fig.3(b), the theoretical result provided by Sengupta and Mitra's method is compared to the experimental singular value distribution but also to the result provided by a numerical simulation. It consists in generating numerically a matrix \mathbf{P} whose elements are circularly symmetric complex gaussian random variables with zero mean. Then, a matrix \mathbf{Q} is built from \mathbf{P} , such that

$$\mathbf{Q} = \hat{\mathbf{C}}^{\frac{1}{2}} \mathbf{P} \hat{\mathbf{C}}^{\frac{1}{2}} \quad (10)$$

One can show that the matrix \mathbf{Q} exhibits the same correlation properties at emission and reception as the experimental matrix \mathbf{K} . A histogram of singular values is obtained by achieving the SVD of \mathbf{Q} , renormalizing its singular values according to Eq.1 and averaging the result over 2000 realizations. The agreement between the numerical and theoretical distributions of singular values is perfect, which illustrates the validity of the theoretical method given in [34]. Taking the correlations into account improves significantly the agreement between theory and experiment.

An interesting result is that the distribution of singular values remains bounded even in presence of correlations. Here, taking Γ_m into account, theoretical results show that the singular values can never exceed $\lambda_{max} = 2.5$. On the contrary, the maximum value predicted by the quarter-circle law (which would apply if the matrix elements were independent and $N \gg 1$) is $\lambda_{max} = 2$. Note that a slight difference between experimental and theoretical results still remains near λ_{max} .

Moreover, because of spatial reciprocity, the matrix \mathbf{K} is symmetric. This property results once again in a deviation from the quarter circle law theorem which assumes independent matrix coefficients [6]. We will consider here the case of the truncated matrix $\tilde{\mathbf{K}}_t$ as defined in Sec.III B, in order to study the effect of symmetry independently from the presence of correlations between adjacent entries. Another numerical simulation is performed. It consists in generating a symmetric matrix \mathbf{P} of dimension $\frac{N}{2} \times \frac{N}{2}$ whose elements are circularly symmetric complex gaussian random variables with zero mean. A histogram of singular values is obtained by computing the SVD of \mathbf{P} , renormalizing its singular values according to Eq.1 and averaging the result over 2000 realizations. The distribution of singular values provided by numerical calculations does not exactly match the quarter circle law (see Fig.5(b)). More precisely, the deviation appears mainly at the boundaries of the theoretical

support of $\rho(\lambda)$, i.e in the vicinity of $\lambda = 0$ and $\lambda = 2$. The reason for this deviation is shown in Appendix C. By and large, the symmetry of \mathbf{K} induces additional correlations between diagonal elements of the autocorrelation matrix $\mathbf{K}\mathbf{K}^\dagger$, which do not exist when the random matrix is not symmetric. These residual correlations are shown to be of the order of $\frac{1}{N}$. In our experimental configuration ($N/2 = 32$), they are quite low but sufficient to induce a slight deviation from the quarter circle law especially near $\lambda = 0$.

E. Conclusion

It appears that in the absence of spatial correlations between matrix entries k_{ij} , the experimental distribution of singular values is close to the quarter circle law. Nevertheless, some deviations from the assumptions generally made in RMT have been pointed out. First, the elements of \mathbf{K} are not identically distributed. The reason for that is the inhomogeneous distribution of backscattered intensity, due to the coherent backscattering enhancement as well as the decreasing of the diffuse halo with the distance between the transmitter and the receiver. Another cause of deviation has been pointed out numerically: the symmetry of the array response matrix, which induces additional correlations between matrix coefficients. All these effects become negligible as long as $N \gg 1$. Yet they slow down the convergence of $\rho(\lambda)$ to the quarter-circle law.

In the presence of correlations between entries, the method proposed by Sengupta and Mitra[34] allows one to calculate the distribution of singular values. As a preliminary conclusion, in the case where multiple scattering dominates, the normalized response matrix $\tilde{\mathbf{K}}$ falls into the general scope of RMT and a theoretical prediction of the singular value spectrum can be achieved. Particularly, an upper bound λ_{max} for the singular values can be calculated. As it will be shown in the next section, this is no longer true if single scattering dominates. Note also that this agreement with classical results of RMT only holds in a diffusive regime. Indeed, if we approach Anderson localization ($kl_e \sim 1$), one can expect that interference effects, such as hot spots [50, 51] or loops [52, 53], should strongly affect the distribution of singular values [11]. Yet in our experimental configuration, we are far from strong localization ($kl_e \sim 100$).

IV. SINGLE-SCATTERING REGIME

In this section, we consider the case of a weakly scattering medium. The sample under investigation is now a slab of gel (composed of 5% of gelatine and 3% of agar-agar), with thickness $L \simeq 100$ mm and a mean free path $l_e \sim 1000$ mm. In such conditions, the multiple scattering contribution is negligible. The array-sample distance a is 60 mm. The experimental procedure and the numerical processing are performed as described in Sec.II. A typical example of a matrix $\tilde{\mathbf{K}}(T, f)$ measured experimentally is given in Fig.6(a). Contrary to the multiple scattering regime, the array response matrix $\tilde{\mathbf{K}}$ exhibits a deterministic coherence along its antidiagonals, although the scatterers distribution in the agar gel is random. We briefly recall the origins of this phenomenon [37] and its impact on the singular values distribution.

As before, the signals $k_{ij}(T, f)$ at a time T and frequency f correspond to the sum of partial waves that reach the array in the time window $[T - \Delta t/2; T + \Delta t/2]$ except that only single-scattering paths are now considered. The *isochronous volume* is defined as the ensemble of points that contribute to the backscattered signal at a given time. It is formed by a superposition of ellipses whose foci are transmitter i and receiver j . In a far-field configuration, we approximate the isochronous volume by a slab of thickness $\Delta r = c\Delta t$, located at a distance $R = cT$ from the array and parallel to it. For simplicity but without loss of generality, we also assume that the reflectors as well as the array elements are point-like.

In a 2D configuration, under the paraxial approximation, $k_{ij}(T, f)$ can be expressed as

$$k_{ij}(T, f) \propto \frac{\exp(j2kR)}{R} \sum_{d=1}^{N_d} A_d \exp \left[jk \frac{(x_i - X_d)^2}{2R} \right] \exp \left[jk \frac{(x_j - X_d)^2}{2R} \right] \quad (11)$$

The index d denotes the d^{th} path which contributes to the signal received at time T . X_d is the transversal position of the reflector associated with this path and the amplitude A_d depends on the reflectivity of the scatterer.

Let us express k_{ij} as a function of variables $(x_i - x_j)$ and $(x_i + x_j)$:

$$k_{ij}(T, f) \propto \underbrace{\frac{\exp(j2kR)}{R} \exp \left[jk \frac{(x_i - x_j)^2}{4R} \right]}_{\text{deterministic term}} \underbrace{\sum_{d=1}^{N_d} A_d \exp \left[jk \frac{(x_i + x_j - 2X_d)^2}{4R} \right]}_{\text{random term}} \quad (12)$$

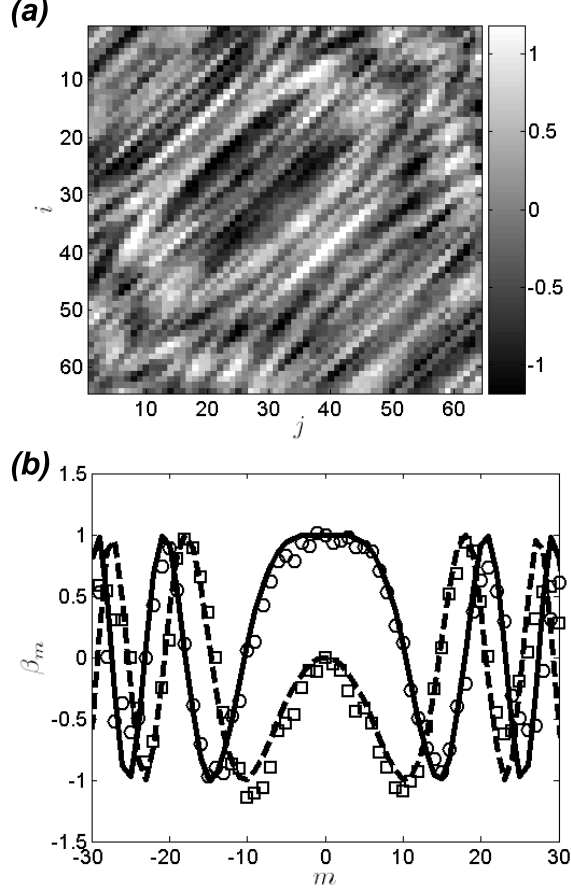


FIG. 6: Experimental results in a single-scattering sample (agar gel). (a) Real part of the matrix $\tilde{\mathbf{K}}(T, f)$ obtained at time $T=265 \mu\text{s}$ and frequency $f=3.1 \text{ MHz}$. (b) Real(white disks) and imaginary(white squares) parts of β_m are shown as a function of m and are compared to the real(continuous line) and imaginary (dashed line) parts of Eq.13.

The term before the sum in Eq.12 does not depend on the scatterers distribution. On the contrary, the term on the right does; hence it is random. As a consequence, single scattering manifests itself as a particular coherence along the antidiagonals of the matrix \mathbf{K} , as illustrated in Fig.6. Indeed, in a given sample, along each antidiagonal (*i.e.* for couples of transmitter i and receiver j such that $i + j$ is constant), the random term of Eq.12 is the same. So, whatever the realization of disorder, there is a deterministic phase relation between coefficients of \mathbf{K} located on the same antidiagonal. It can be written as:

$$\beta_m = \frac{k_{i-m, j+m}(T, f)}{k_{ii}(T, f)} = \exp \left[jk \frac{(mp)^2}{R} \right] \quad (13)$$

Note that this essential result is valid independently of the scatterers configuration, under

two conditions: single scattering and paraxial approximation. The parabolic phase dependence along each antidiagonal predicted by Eq.13 is compared in Fig.6(b) with the coefficient β_m obtained experimentally at time $T = 265 \mu s$ and frequency $f = 3.1$ MHz along the main antidiagonal (*i.e* $i = 32$). Theoretical and experimental results are in a very good agreement.

In order to investigate independently the effect of the deterministic coherence along antidiagonals of $\tilde{\mathbf{K}}$, other correlations that may exist between lines and columns of the matrix \mathbf{K} have to be removed. These correlations are measured by assessing the normalized correlation coefficient Γ_m (Eq.3). Γ_m (not shown here) spreads until $|m| = 2$ for this experiment. Thus, the initial set of matrices $\mathbf{K}(T, f)$ has been truncated by keeping only one in three elements. Note that only correlations between lines and columns of \mathbf{K} are cleared. The deterministic coherence along antidiagonals is long-range and hence is not removed by this operation. As before, the truncated matrix $\mathbf{K}_t(T, f)$ is renormalized (Eq.1). The experimental distribution of singular values is shown in Fig.7: clearly, it does not follow the quarter circle law, even though correlations between neighbouring entries have been removed. This

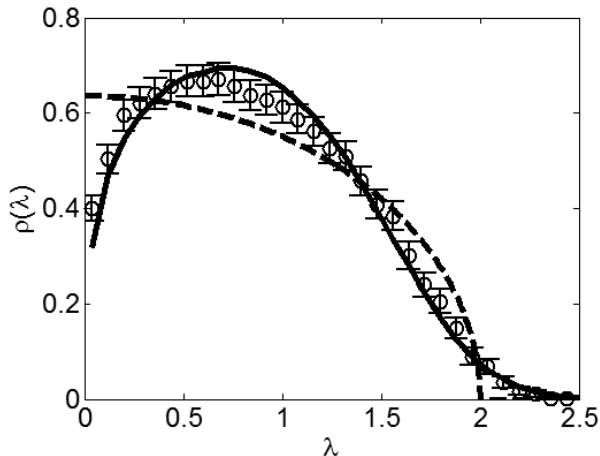


FIG. 7: The experimental distribution of singular values $\hat{\rho}(\lambda)$ in the single-scattering case (white disks) is compared to the quarter circle law $\rho_{QC}(\lambda)$ (dashed curve) and to the the Hankel law $\rho_H(\lambda)$ (continuous curve) which has been calculated numerically. The error bars are \pm two standard deviations.

is due to the deterministic coherence of single scattered signals along the antidigonals of $\tilde{\mathbf{K}}_t$.

To our knowledge, this kind of random matrix whose antidiagonal elements are linked with a deterministic phase relation have not been yet investigated theoretically. But its

properties are close to those of a random Hankel matrix, whose spectral behaviour has been studied recently[54]. A Hankel matrix is a $N \times N$ square matrix whose elements belonging to the same antidiagonal ($i + j = \text{constant}$) are equal. Let $\{a_p\}$ be a sequence of $2N - 1$ complex random variables identically and independently distributed with zero mean. The Hankel matrix \mathbf{R} built such as $r_{ij} = a_{i+j-1}$, is said random. We have checked numerically that a random matrix whose antidiagonal elements are linked with a deterministic phase relation displays the same singular value distribution as a Hankel random matrix, provided that all elements of this matrix are zero mean and have the same variance. In the literature, Bryc *et al.* [54] have proved, for normalized random Hankel matrices, the almost sure weak convergence of the distribution of eigenvalues to a universal, non random, symmetric distribution of unbounded support. We will assume that this convergence property also applies to the singular values distribution of a random Hankel matrix. In the following, $\rho_H(\lambda)$ will denote the asymptotic singular values distribution of a random Hankel matrix and will be referred to as the Hankel law. To our knowledge, no analytical expression of the Hankel law has been found yet and only a numerical calculation can provide an estimate of $\rho_H(\lambda)$. In Fig.7, the experimental distribution of singular values of $\tilde{\mathbf{K}}_t$ has been compared to the Hankel law. $\rho_H(\lambda)$ is provided by a numerical generation of random Hankel matrices. The agreement between both curves is excellent. An important feature of the Hankel law is its unbounded support. As a consequence, in the single scattering regime, the first singular value has no bound, contrary to the multiple scattering case for which the first singular value could never be higher than λ_{max} in the asymptotic limit ($N \rightarrow \infty$). This difference of behaviour is crucial when one wants to detect a target embedded in a random scattering medium, as we discuss in the next section.

V. DETECTION OF A TARGET EMBEDDED IN A RANDOM MEDIUM

The configuration we consider is the same as in Fig.1, except that a target (a stronger reflector) may be embedded in the scattering medium. The issue is to detect its presence from the SVD of the \mathbf{K} matrix: if the strongest normalized singular value $\tilde{\lambda}_1$ is above a certain threshold α , we will conclude (with a certain probability of error) that there is indeed a target. Assume the occurrence of a target at a depth R . The array response matrix

$\mathbf{K}(T, f)$ at the time of flight $T = 2R/c$ can be written as :

$$\mathbf{K}(T, f) = \mathbf{K}^T(T, f) + \mathbf{K}^R(T, f) \quad (14)$$

$\mathbf{K}^T(T, f)$ is the contribution of the direct echo reflected by the target, and $\mathbf{K}^R(T, f)$ the response of the random medium, which may include single scattering, multiple scattering contributions as well as additive noise. $\mathbf{K}^R(T, f)$ can be seen as a perturbation (not necessarily small) of $\mathbf{K}^T(T, f)$. As usual, the matrix is renormalized according to Eq.1. For simplicity, we will assume that short-range correlations have been removed, so that the relevant probability density function of the singular values of \mathbf{K}^R should be the quarter-circle law (for $N \gg 1$ in the multiple scattering regime) and the Hankel law (in the single scattering regime).

In a first approximation, \mathbf{K}^T is of rank 1 (actually, for a resonant or a large target \mathbf{K}^T may have more than one significant singular value [55, 56, 57, 58, 59]). \mathbf{K}^R is random, and its normalized singular values have a probability density $\rho^R(\lambda)$. Depending on the scattering properties of the medium (particularly, its mean-free path), at time $T = 2R/c$, $\rho^R(\lambda)$ may follow the Hankel law (if single scattering dominates), the quarter-circle law (if multiple scattering or additive noise dominate) or a combination of both in intermediate situations. Let $\tilde{\lambda}_1^R$ denote the highest singular value of $\tilde{\mathbf{K}}^R(T, f)$. As a detection threshold based on the first singular value of \mathbf{K} is needed, the statistical behavior of $\tilde{\lambda}_1^R$ has to be known. If the singular values of $\mathbf{K}^R(T, f)$ were independent from each other, then the distribution function F_1^R of $\tilde{\lambda}_1^R$ would be simply given by the N^{th} power of the distribution function $F^R(\lambda)$ of one singular value, with

$$F^R(\lambda) = \int_0^\lambda dx \rho^R(x).$$

Actually, the singular values of a random matrix are not independent because of level repulsion [60, 61]. It implies a zero probability for degenerate singular spaces: the singular values tend to keep away from each other. Thus, the probability density function $\rho_1^R(\lambda)$ and the distribution function $F_1^R(\lambda)$ of the first singular value $\tilde{\lambda}_1^R$ cannot be deduced simply from $\rho^R(\lambda)$.

Once again, we will refer to RMT and particularly to the theoretical studies dealing with the first eigenvalue of the autocorrelation matrix $\mathbf{K}^R \mathbf{K}^{R\dagger}$, *i.e.* $\left[\tilde{\lambda}_1^R\right]^2$. If \mathbf{K}^R is a “classical”

random matrix (multiple scattering regime), $\left[\tilde{\lambda}_1^R\right]^2$ is given by [35, 62, 63, 64, 65]:

$$\left[\tilde{\lambda}_1^R\right]^2 = 4 + \left(\frac{N}{4}\right)^{-\frac{2}{3}} Z + o\left(N^{-\frac{2}{3}}\right) \quad (15)$$

where Z is a random variable whose probability density function is a complicated law, known as the *Tracy Widom* distribution. It is an asymmetric bell curve, uncentered and of infinite support [62, 63]. No analytic expression is available, nevertheless it can be estimated numerically. In our case, we are rather interested in the density of probability ρ_1^R of the first singular value $\tilde{\lambda}_1^R$. ρ_1^R has been estimated by generating numerically “classical” random matrices and is displayed in Fig.8(a), for $N = 32$ and $N = 100$. Although the quarter circle law ρ_{QC} is of bounded support, ρ_1^R is of infinite support. Indeed, ρ_{QC} is only an asymptotic law, *i.e* valid for $N \rightarrow \infty$. For a random matrix of finite dimension, $\tilde{\lambda}_1^R$ has a non zero probability of exceeding $\lambda_{\max} = 2$. Nevertheless, $\rho_1^R(\lambda)$ narrows with N : the variance of $\tilde{\lambda}_1^R$ decreases when N grows, and its expected value has been shown to be bounded by $\lambda_{\max} = 2$.

The relevant quantity for the detection issue is the distribution function F_1^R of the first singular value $\tilde{\lambda}_1^R$. F_1^R is the primitive of ρ_1^R ,

$$F_1^R(\lambda) = P\left\{\tilde{\lambda}_1^R \leq \lambda\right\} = \int_0^\lambda dx \rho_1^R(x).$$

In terms of target detection, the probability of false alarm is $PFA(\alpha) = 1 - F_1^R(\alpha)$. By setting an acceptable PFA , we can determine the corresponding threshold above which a target is said to be detected. The distribution functions F_1^R , for $N = 32$ and $N = 100$, are plotted in Fig.8(b). In the multiple scattering regime (“classical” random matrix), we observe that, for $N = 32$ and $N = 100$, $F_1^R(\lambda = 2) \simeq 0,99$: if the PFA is fixed at 1%, $\alpha = 2$ is the corresponding threshold.

This is no longer the case if the propagation operator behaves as a Hankel matrix (single scattering regime): the threshold is much higher, making the detection more difficult, for the same PFA . Theoretical results indicate that the expected value of the first singular value grows as $\sqrt{\log(N)}$ [66]. This is illustrated in Fig.8: ρ_1^R and F_1^R have been calculated by generating numerically random Hankel matrices for $N = 32$ and $N = 100$. As N is enlarged the curves are shifted towards right, which implies a larger probability of false alarm for a given detection threshold α . Other theoretical studies have shown that the fluctuations of

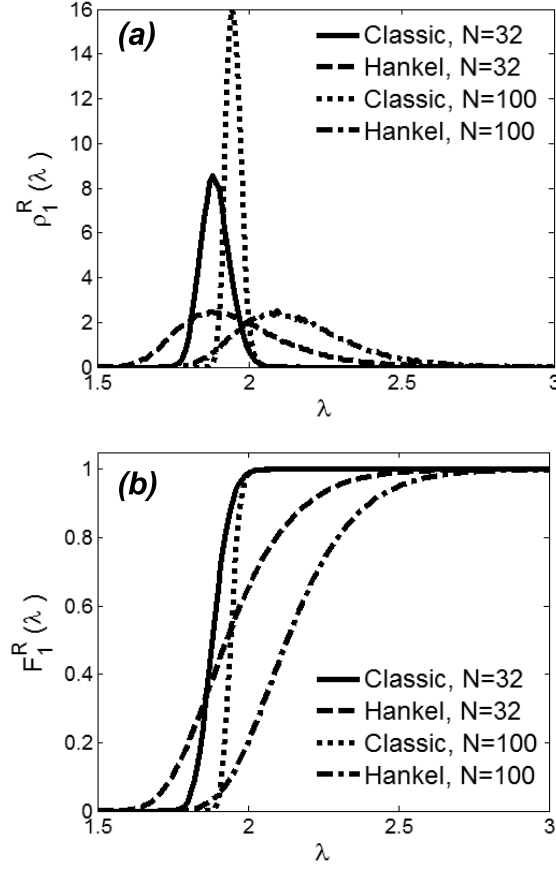


FIG. 8: (a) Probability density function ρ_1^R of the first singular value $\tilde{\lambda}_1^R$ estimated numerically. The multiple scattering case corresponds to continuous ($N = 32$) and dotted ($N = 100$) curves. The single-scattering case corresponds to dashed ($N = 32$) and dash-dotted ($N = 100$) curves. (b) Distribution function $F_1^R(\lambda)$ of the first singular value $\tilde{\lambda}_1^R$. The multiple-scattering case still corresponds to continuous ($N = 32$) and dotted ($N = 100$) curves. The single-scattering case corresponds to dashed ($N = 32$) and dash-dotted ($N = 100$) curves.

$\tilde{\lambda}_1^R$ are inferior to $\sqrt{\log N}$ [67] and that, in the gaussian case, the variance of $\tilde{\lambda}_1^R$ remains bounded [68].

In a real situation, single and multiple scattering coexist; what is the relevant distribution function F_1^R ? If multiple scattering dominates (*i.e.*, the target depth is larger than a few mean-free paths) or if the perturbation \mathbf{K}^R is additive uncorrelated noise, the probability of false alarm $PFA(\alpha) = 1 - F_1^R(\alpha)$ is deduced considering the distribution function F_1^R obtained for a “classical” random matrix. If no *a priori* information is available regarding the scattering medium, we have to calculate F_1^R for a “classical” random matrix and for a

random Hankel matrix, deduce two values for the probability of false alarm $1 - F_1^R(\alpha)$, and keep the highest.

In the view of applications (*e.g.*, non-destructive evaluation, target detection *etc.*) an acceptable probability of false alarm P_0 is set first, hence the detection threshold :

$$\alpha = F_1^{-1}(1 - P_0) \quad (16)$$

Once the usual normalization is performed, if $\tilde{\lambda}_1 > \alpha$ a target is detected at time T and frequency f . Conversely, if $\tilde{\lambda}_1 < \alpha$ one cannot conclude about the possible presence of a target.

The detection criterion (Eq.16) can be used to estimate the performance of the DORT method in a random medium (or in the presence of noise). Let σ_T^2 and σ_R^2 be the power of signals associated with the target and the random contribution. If the first singular value λ_1 of \mathbf{K} is associated to the target echo, then the expected value of λ_1 is λ_1^T . In Appendix D, we show that $\lambda_1^T = N\sigma_T$, so

$$\mathbb{E} \{ \lambda_1 \} = N\sigma_T.$$

We also show in Appendix D that the quadratic mean of the singular values can be expressed as

$$\sqrt{\frac{1}{N} \sum_{p=1} \lambda_p^2} = \sqrt{N(\sigma_T^2 + \sigma_R^2)}.$$

Upon normalization, we have

$$\mathbb{E} \{ \tilde{\lambda}_1 \} = \sqrt{N \frac{\sigma_T^2}{\sigma_T^2 + \sigma_R^2}} \simeq \frac{\sigma_T}{\sigma_R} \sqrt{N}, \text{ for } \sigma_T^2 \ll \sigma_R^2$$

and $\text{var} \{ \tilde{\lambda}_1 \} \simeq \frac{1}{2}$. Even though the echo of the target may be very weak compared to the scattering contribution, DORT can be expected to detect it if $\tilde{\lambda}_1 > \alpha$, *i.e.*,

$$\frac{\sigma_T}{\sigma_R} > \frac{F_1^{-1}(1 - P_0)}{\sqrt{N}}. \quad (17)$$

The most favourable situation is when the quarter-circle law is valid (multiple scattering regime or additive white noise, and $N \gg 1$) : in that case α can be fixed to 2, which corresponds for $N = 32$ to a probability of false alarm $P_0 \simeq 1\%$, and typically the target will be detected if

$$\frac{\sigma_T}{\sigma_R} > \frac{2}{\sqrt{N}}. \quad (18)$$

In other words, the weakness of the target may be compensated by an increasing number of array elements: the performance of the DORT method is improved as the square-root of the number of independent channels. However in the single scattering regime, the expected value of $\tilde{\lambda}_1^R$ grows as $\sqrt{\log N}$ [66]. For a given P_0 , we can assume that α increases also as $\sqrt{\log N}$. Hence, the performance of the D.O.R.T method grows as $\sqrt{\frac{N}{\log N}}$, which is significantly slower than \sqrt{N} .

VI. CONCLUSION

In this article, the distribution of singular values of the array response matrix \mathbf{K} in a random medium has been investigated, in a backscattering configuration. Once a judicious renormalization is achieved, the distribution $\rho(\lambda)$ obtained experimentally with ultrasonic waves in scattering samples is in very good agreement with theoretical predictions. Interestingly, $\rho(\lambda)$ is shown to differ significantly in the single and multiple scattering regimes. When multiple scattering dominates, as long as spatial correlations between matrix entries are negligible, $\rho(\lambda)$ is found to approach the quarter circle law. Correlations between matrix entries can also be taken into account: in that case, $\rho(\lambda)$ can be calculated following the method proposed by Sengupta and Mitra[34]. On the contrary, single scattering contributions exhibit a different behaviour: whatever the realisation of disorder, a deterministic coherence persists along each antidiagonal of the matrix \mathbf{K} . As a consequence, $\rho(\lambda)$ no longer follows the quarter-circle law and the singular spectrum of \mathbf{K} becomes analogous to that of a Hankel matrix. These results have been applied to the detection of a target embedded in a random scattering media. Once the matrix is renormalized, knowing the distribution $\rho(\lambda)$ allows one to define a rigorous detection criterion based on the strongest singular value, which is expected to be associated to the target. The perspectives of this work are many. The results could be applied to all fields of wave physics where coherent transmit/receive arrays are available for imaging and detection (*e.g.*, non destructive testing of scattering materials, underwater acoustics, landmine detection, seismology, radar/sonar, *etc.*)

VII. ACKNOWLEDGMENTS

The authors wish to acknowledge Josselin Garnier, Arnaud Tourin, Claire Prada, Julien de Rosny and Mathias Fink for fruitful discussions. They also wish to acknowledge the groupe de recherches IMCODE of CNRS (GDR 2253), Patricia Daenens for her technical help and Victor Mamou who made the steel rods samples.

APPENDIX A:

The time-window length Δt is chosen so that signals associated with the same scattering path within the medium are in the same time window. For the sake of simplicity, here we only deal with single scattering paths but we would obtain the same results if multiple-scattering paths were considered.

To calculate Δt , we have to find the two single-scattering paths, associated to the same scattering event, for which the difference of travel length is the highest. To that aim, the directivity of transducers has to be taken into account. The major part of the energy is transmitted (received) towards (from) scatterers located into a cone whose aperture is $2\theta_{max}$. When the response k_{ij} is considered, only the scatterers contained inside the volume common to the directivity cones of elements i and j have to be considered.

At each depth Z_s , we have to optimize the lateral position X_s of the scatterer which results in the largest difference of travel length between two single-scattering paths. These paths are associated with two source/receiver couples (i, j) and (l, m) . Thus, we have to optimize simultaneously the position X_s , and the couples (i, j) and (l, m) . This issue can be simplified because we have to deal with single-scattering paths. Because of the equivalence of the forward and return waves, source and receiver of each couples are in fact identical. So, we have to find the elements i and l which are respectively the furthest and the nearest elements from the scatterer whose coordinates are (X_s, Z_s) , X_s remaining unknown. The result of this optimization differs according to the depth Z_s of the scatterer :

- $Z_s < Z_{lim} = \frac{D}{2} \cos \theta_{max}$: the two paths s_1 and s'_1 corresponding to the largest difference of travel length are shown with dashed arrows in Fig.9. s_1 is the longest path and contributes to the signal k_{11} . It is linked with a scatterer which is located on the top generatrix of the directivity cone of the first transducer. s'_1 is the shortest path. It is

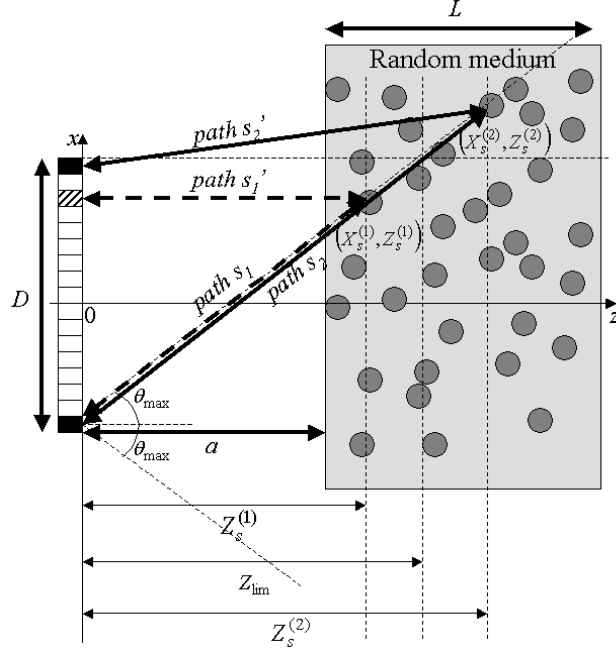


FIG. 9: Choice of the appropriate time-window length Δt . The single scattered paths s and s' are associated with the reflection on the same scatterer. Two situations can occur. The case $z = Z_s^{(1)}$, when $Z_s^{(1)} < Z_{lim}$, corresponds to the dashed arrows. The two paths s_1 and s'_1 have been chosen so that the difference of travel length is the largest. In the case $z = Z_s^{(2)}$ (with $Z_s^{(2)} > Z_{lim}$), continuous arrows represent the two paths s_2 and s'_2 for which the difference of travel length is the largest.

associated with the p^{th} element of the array and thus contributes to the signal k_{pp} . The transducer p is at the same transverse position X_s as the scatterer. So, for $Z_s < Z_{lim}$, Δt is then given by

$$\Delta t = \frac{2Z_s}{c} \left[\frac{1}{\cos \theta_{max}} - 1 \right] \quad (A1)$$

- $Z_s > Z_{lim}$: the two paths s_2 and s'_2 are depicted with continuous arrows in Fig.9. As previously, s_2 is the longest path and contributes to the signal k_{11} . It is still linked with a scatterer which is located on the top generatrix of the directivity cone of the first transducer. s'_2 is the shortest path. It is associated with the N^{th} element of the array and thus contributes to the signal k_{NN} . For $Z_s > Z_{lim}$, Δt is hence given by

$$\Delta t = \frac{2}{c} \left[\frac{Z_s}{\cos \theta_{max}} - \sqrt{(Z_s \tan \theta_{max} + D)^2 + Z_s^2} \right] \quad (A2)$$

where D is the array aperture. When $Z_s \rightarrow \infty$, Eq.A2 becomes

$$\lim_{Z_s \rightarrow +\infty} \Delta t = \frac{2D \sin \theta_{max}}{c} \quad (\text{A3})$$

In practice, we have to assess Δt by considering the maximum depth $Z_{max} = a + L$. For the experiment described in Sec.III, $Z_{max} = 65$ mm. Considering an aperture angle $\theta_{max} = 27.5$ deg, we obtain a value $\Delta t \simeq 10\mu s$. For the experiment described in Sec.IV, $Z_{max} = 150$ mm. Thus the value Δt should be fixed to $14\mu s$. Nevertheless, given the finite width of the agar gel sample (8 cm), there is no need to use such long temporal windows and a time-window length $\Delta t = 10\mu s$ is also considered.

APPENDIX B:

As seen in Sec.III C, the coherent backscattering effect arises in the diagonal of matrix $\tilde{\mathbf{K}}$: the variance of coefficients \tilde{k}_{ii} is twice that of off-diagonal elements. We want to estimate the influence of the coherent backscattering effect on the singular values distribution. To that aim, we will investigate its influence on the statistical properties of the autocorrelation matrix.

Let us first consider a random matrix \mathbf{R} of dimension $N \times N$. We assume that the coefficients of the matrix \mathbf{R} are complex gaussian random variables *i.i.d*, with a zero-mean and a variance of $1/N$. The theoretical singular values distribution of a random matrix \mathbf{R} (the quarter circle law) is deduced directly from the eigenvalues distribution of the autocorrelation matrix $\mathbf{A} = \mathbf{R}\mathbf{R}^\dagger$ (the so-called Marčenko-Pastur law [6]), since singular values of \mathbf{R} correspond to the square root of eigenvalues of $\mathbf{A} = \mathbf{R}\mathbf{R}^\dagger$. We now focus on the statistical properties of \mathbf{A} . The entries a_{lm} of matrix \mathbf{A} are given by

$$a_{lm} = \sum_{p=1}^N r_{lp} r_{mp}^* \quad (\text{B1})$$

Let us calculate the mean and the variance of coefficients a_{lm} . $\langle a_{lm} \rangle$ is given by

$$\begin{aligned} \langle a_{lm} \rangle &= \sum_{p=1}^N \langle r_{lp} r_{mp}^* \rangle \\ \langle a_{lm} \rangle &= \begin{cases} 0 & \text{if } l \neq m \\ \sum_{p=1}^N \langle |r_{lp}|^2 \rangle = 1 & \text{otherwise} \end{cases} \end{aligned}$$

The mean of coefficients a_{lm} is not nil only for diagonal elements

$$\langle a_{lm} \rangle = \delta_{lm} \quad (\text{B2})$$

$\langle |a_{lm}|^2 \rangle$ can be developed as

$$\langle |a_{lm}|^2 \rangle = \sum_{p=1}^N \sum_{q=1}^N \langle r_{lp} r_{mp}^* r_{lq}^* r_{mq} \rangle$$

Using the moment theorem, $\langle |a_{lm}|^2 \rangle$ becomes

$$\langle |a_{lm}|^2 \rangle = \underbrace{\sum_{p=1}^N \sum_{q=1}^N \langle r_{lp} r_{mp}^* \rangle \langle r_{lq}^* r_{mq} \rangle}_{|\langle a_{lm} \rangle|^2} + \underbrace{\sum_{p=1}^N \sum_{q=1}^N \langle r_{lp} r_{lq}^* \rangle \langle r_{mp}^* r_{mq} \rangle}_{\text{var}[a_{lm}]} \quad (\text{B3})$$

To calculate $\text{var}[a_{lm}]$, we use the fact that

$$\langle r_{lp} r_{lq}^* \rangle = \frac{1}{N} \delta_{pq}$$

We obtain

$$\text{var}[a_{lm}] = \frac{1}{N^2} \sum_{p=1}^N \sum_{q=1}^N \delta_{pq} = \frac{1}{N} \quad (\text{B4})$$

Finally, the off-diagonal entries of \mathbf{A} are complex random variables with zero mean and variance $1/N$. The diagonal elements of \mathbf{A} are also complex random variables but with a mean equal to 1 and a variance of $1/N$.

Now that we have calculated the mean and variance of the autocorrelation coefficients a_{lm} built from a “classical” random matrix \mathbf{R} , we focus on the effect of coherent backscattering. To that aim, we consider the matrix $\tilde{\mathbf{K}}$ which is obtained experimentally in the multiple scattering regime. This matrix is built from the array response matrix \mathbf{K} :

$$\tilde{k}_{ij} = \frac{k_{ij}}{\sqrt{\frac{1}{N} \sum_{p=1}^N \sum_{q=1}^N |k_{pq}|^2}} \quad (\text{B5})$$

Eq.B5 is another expression for the renormalization presented in Eq.1. By construction, we have

$$\frac{1}{N} \sum_{i=1}^N \sum_{j=1}^N |\tilde{k}_{ij}|^2 = 1 \quad (\text{B6})$$

Note that the random matrix \mathbf{R} verifies the same property. But, as pointed out in Sec.III C, the variance of elements of $\tilde{\mathbf{K}}$ is not constant. In particular, the matrix $\tilde{\mathbf{K}}$ exhibits a double

variance along its diagonal because of the coherent backscattering phenomenon. To estimate its effect on the singular value spectrum, we model $\tilde{\mathbf{K}}$ as a matrix whose coefficients \tilde{k}_{ij} are complex gaussian random variables independently distributed with mean zero and a variance σ_{ij}^2 defined as

$$\sigma_{ij}^2 = \begin{cases} \sigma^2 & \text{if } i \neq j \\ 2\sigma^2 & \text{if } i = j \end{cases} \quad (\text{B7})$$

Eq.B6 leads to

$$\begin{aligned} \frac{1}{N^2} \sum_{p=1}^N \sum_{q=1}^N \sigma_{pq}^2 &= \frac{1}{N} \\ \frac{1}{N^2} \sum_{p=1}^N [(N-1)\sigma^2 + 2\sigma^2] &= \frac{1}{N} \\ \frac{N(N+1)}{N^2} \sigma^2 &= \frac{1}{N}, \end{aligned}$$

which yields

$$\sigma^2 = \frac{1}{N+1} \quad (\text{B8})$$

σ_{ij}^2 is finally given by

$$\sigma_{ij}^2 = \frac{1 + \delta_{ij}}{N+1} \quad (\text{B9})$$

The variance of elements \tilde{k}_{ij} is equal to $\frac{1}{N+1}$ for off-diagonal elements ($i \neq j$) and twice for diagonal elements ($i = j$).

Let us focus now on the autocorrelation matrix $\mathbf{B} = \tilde{\mathbf{K}}\tilde{\mathbf{K}}^\dagger$. Its coefficients are defined as

$$b_{lm} = \sum_{p=1}^N \tilde{k}_{lp} \tilde{k}_{mp}^* \quad (\text{B10})$$

The mean of coefficients b_{lm} is given by

$$\begin{aligned} \langle b_{lm} \rangle &= \sum_{p=1}^N \langle \tilde{k}_{lp} \tilde{k}_{mp}^* \rangle \\ \langle b_{lm} \rangle &= \begin{cases} 0, & \text{if } l \neq m \\ \sum_{p=1}^N \langle |\tilde{k}_{lp}|^2 \rangle = \sigma_{ll}^2 + \sum_{p \neq l}^N \sigma_{lp}^2 = \frac{2}{N+1} + \frac{N-1}{N+1} = 1, & \text{otherwise} \end{cases} \end{aligned}$$

We obtain the same mean for b_{lm} as for a_{lm} (Eq.B2)

$$\langle b_{lm} \rangle = \delta_{lm} \quad (\text{B11})$$

As to the variance of coefficient b_{lm} , it can be expressed as

$$\begin{aligned}
\text{var}[b_{lm}] &= \sum_{p=1}^N \sum_{q=1}^N \underbrace{\langle \tilde{k}_{lp} \tilde{k}_{lq}^* \rangle}_{\sigma_{lq}^2 \delta_{pq}} \underbrace{\langle \tilde{k}_{mp}^* \tilde{k}_{mq} \rangle}_{\sigma_{mq}^2 \delta_{pq}} \\
\text{var}[b_{lm}] &= \sum_{q=1}^N \sigma_{lq}^2 \sigma_{mq}^2 \\
\text{var}[b_{lm}] &= \frac{1}{(N+1)^2} \sum_{q=1}^N (1 + \delta_{lq})(1 + \delta_{mq}) \\
\text{var}[b_{lm}] &= \frac{1}{(N+1)^2} (N + 2 + \delta_{lm}) \\
\text{var}[b_{lm}] &= \frac{N + 2 + \delta_{lm}}{(N+1)^2} \tag{B12}
\end{aligned}$$

The statistical properties of the autocorrelation matrices \mathbf{A} and \mathbf{B} are summed up in Tab.I. The coherent backscattering effect increases the variance of the autocorrelation coefficients,

“Classical” random matrix \mathbf{R}	Experimental matrix $\tilde{\mathbf{K}}$
$\mathbf{A} = \mathbf{R}\mathbf{R}^\dagger$	$\mathbf{B} = \tilde{\mathbf{K}}\tilde{\mathbf{K}}^\dagger$
$\langle a_{lm} \rangle = \delta_{lm}$	$\langle b_{lm} \rangle = \delta_{lm}$
$\text{var}[a_{lm}] = \frac{1}{N}$	$\text{var}[b_{lm}] = \frac{N+2+\delta_{lm}}{(N+1)^2}$

TABLE I: Statistical properties of autocorrelation matrices \mathbf{A} and \mathbf{B} , depending on whether the initial matrix exhibits the coherent backscattering effect or not.

compared to the *classical case*. Thus, the eigenvalues spectrum of the autocorrelation matrix and also the singular values distribution of $\tilde{\mathbf{K}}$ should be modified by the coherent backscattering effect. But, for $N \gg 1$, the difference between $\frac{1}{N}$, $\frac{N+2}{(N+1)^2}$ and $\frac{N+3}{(N+1)^2}$ becomes negligible. For instance, the relative error is about 3% for $N = 32$. So, the double variance of diagonal elements of $\tilde{\mathbf{K}}$ does not perturb significantly the singular values distribution.

APPENDIX C:

We investigate the influence of reciprocity on the statistical properties of the autocorrelation matrix. We will consider first the case of a “classical” random matrix and study the statistical properties of its autocorrelation matrix. The case of a symmetric random matrix

will be studied afterwards. The comparison of the results obtained in both cases will allow us to explain and quantify the influence of symmetry on the singular values distribution. As we will see, the symmetry implies correlations between the diagonal elements of the autocorrelation matrix.

Let us first consider a random matrix \mathbf{R} of dimension $N \times N$. We assume that the coefficients of the matrix \mathbf{R} are complex gaussian random variables *i.i.d*, zero-mean and with variance $1/N$. The entries a_{lm} of the autocorrelation matrix $\mathbf{A} = \mathbf{R}\mathbf{R}^\dagger$ are given by

$$a_{lm} = \sum_{p=1}^N r_{lp} r_{mp}^*$$

Let us calculate the correlation coefficient Θ_{lm}^A between diagonal elements a_{ll} and a_{mm} , which is defined as

$$\Theta_{lm}^A = \frac{\langle a_{ll} a_{mm}^* \rangle - |\langle a_{ll} \rangle|^2}{\text{var}[a_{ll}]} \quad (\text{C1})$$

The correlation term $\langle a_{ll} a_{mm}^* \rangle$ can be developed as

$$\langle a_{ll} a_{mm}^* \rangle = \sum_{p=1}^N \sum_{q=1}^M \langle r_{lp} r_{lp}^* r_{mq} r_{mq}^* \rangle$$

Using the moment theorem, the last equation becomes

$$\langle a_{ll} a_{mm}^* \rangle = \underbrace{\sum_{p=1}^N \sum_{q=1}^M \langle r_{lp} r_{lp}^* \rangle \langle r_{mq} r_{mq}^* \rangle}_{|\langle a_{ll} \rangle|^2} + \sum_{p=1}^N \sum_{q=1}^M \langle r_{lp} r_{mq}^* \rangle \langle r_{mq} r_{lp}^* \rangle \quad (\text{C2})$$

The second sum can be calculated using the fact that

$$\langle r_{lp} r_{mq}^* \rangle = \frac{\delta_{lm} \delta_{pq}}{N} \quad (\text{C3})$$

which yields

$$\begin{aligned} \langle a_{ll} a_{mm}^* \rangle - |\langle a_{ll} \rangle|^2 &= \sum_{p=1}^N \sum_{q=1}^M \frac{\delta_{lm} \delta_{pq}}{N^2} \\ \langle a_{ll} a_{mm}^* \rangle - |\langle a_{ll} \rangle|^2 &= \frac{\delta_{lm}}{N} \end{aligned}$$

Using the fact that $\text{var}[a_{ll}] = \frac{1}{N}$ (Eq.B4), the correlation coefficient Θ_{lm}^A (Eq.C1) is given by

$$\Theta_{lm}^A = \delta_{lm} \quad (\text{C4})$$

This last equation means that the diagonal elements a_{ll} of \mathbf{A} are totally decorrelated from each other.

We now consider the case of a random but symmetric matrix like $\tilde{\mathbf{K}}$. Its coefficients are complex gaussian random variables identically distributed, with mean zero and variance $1/N$. The only difference with a “classical” random matrix \mathbf{R} is the fact that $\tilde{k}_{ij} = \tilde{k}_{ji}$. We neglect here the coherent backscattering effect (see Appendix B) in order to focus on the influence of reciprocity.

Let us study the statistical properties of the autocorrelation matrix $\mathbf{B} = \tilde{\mathbf{K}}\tilde{\mathbf{K}}^\dagger$. One can show that symmetry has no effect on the mean and the variance of b_{lm}

$$\begin{aligned}\langle b_{lm} \rangle &\equiv \langle a_{lm} \rangle = \frac{\delta_{lm}}{N} \\ \text{var}[b_{lm}] &\equiv \text{var}[a_{lm}] = \frac{1}{N}\end{aligned}$$

As done previously for the matrix \mathbf{A} , we define the correlation coefficient Θ_{lm}^B between diagonal elements b_{ll} and b_{mm}

$$\Theta_{lm}^B = \frac{\langle b_{ll}b_{mm}^* \rangle - |\langle b_{ll} \rangle|^2}{\text{var}[b_{ll}]} \quad (\text{C5})$$

The correlation term $\langle b_{ll}b_{mm}^* \rangle$ can be developed as

$$\langle b_{ll}b_{mm}^* \rangle = \sum_{p=1}^N \sum_{q=1}^M \left\langle \tilde{k}_{lp}\tilde{k}_{lp}^* \tilde{k}_{mq}\tilde{k}_{mq}^* \right\rangle$$

Using the moment theorem, the last equation becomes

$$\langle b_{ll}b_{mm}^* \rangle = \underbrace{\sum_{p=1}^N \sum_{q=1}^M \left\langle \tilde{k}_{lp}\tilde{k}_{lp}^* \right\rangle \left\langle \tilde{k}_{mq}\tilde{k}_{mq}^* \right\rangle}_{|\langle b_{ll} \rangle|^2} + \sum_{p=1}^N \sum_{q=1}^M \left\langle \tilde{k}_{lp}\tilde{k}_{mq}^* \right\rangle \left\langle \tilde{k}_{mq}\tilde{k}_{lp}^* \right\rangle$$

But, because $\tilde{k}_{lp} = \tilde{k}_{pl}$, we have

$$\left\langle \tilde{k}_{lp}\tilde{k}_{mq}^* \right\rangle = \frac{\delta_{lm}\delta_{pq}}{N} + \frac{\delta_{lq}\delta_{mp}}{N} \quad (\text{C6})$$

We obtain:

$$\langle b_{ll}b_{mm}^* \rangle - |\langle b_{ll} \rangle|^2 = \frac{\delta_{lm}}{N} + \frac{1}{N^2}$$

Using the fact that $\text{var}[b_{ll}] = \frac{1}{N}$, the correlation coefficient Θ_{lm}^B (Eq.C5) is finally given by

$$\Theta_{lm}^B = \delta_{lm} + \frac{1}{N} \quad (\text{C7})$$

This last equation means that a correlation exists between the diagonal elements b_{ll} of \mathbf{B} , due to reciprocity. The correlations between diagonal elements of matrices \mathbf{A} and \mathbf{B} are compared in Tab.II Even if this correlation is not too large ($1/N \simeq 3\%$ with $N = 32$), it

“Classical” random matrix \mathbf{R}	Symmetric random matrix $\tilde{\mathbf{K}}$
$\mathbf{A} = \mathbf{R}\mathbf{R}^\dagger$	$\mathbf{B} = \tilde{\mathbf{K}}\tilde{\mathbf{K}}^\dagger$
$\Theta_{lm}^A = \delta_{lm}$	$\Theta_{lm}^B = \delta_{lm} + \frac{1}{N}$

TABLE II: Correlation between diagonal elements of autocorrelation matrices \mathbf{A} and \mathbf{B} , depending on whether the initial matrix is symmetric or not.

has an influence on the eigenvalue spectrum of the autocorrelation matrix, hence on the singular values distribution of the matrix $\tilde{\mathbf{K}}$. This explains partly the deviation from the quarter circle law, which we pointed out numerically (see Fig.5(b)). Note that for $N \gg 1$, the influence of symmetry should vanish.

APPENDIX D:

We assume that the matrix \mathbf{K}^T associated to the target is of rank 1. λ_1^T is the only non-zero singular value of \mathbf{K}^T . The trace of the autocorrelation matrix $\mathbf{K}^T\mathbf{K}^{T\dagger}$ can then be expressed as

$$\text{Trace} \left[\mathbf{K}^T\mathbf{K}^{T\dagger} \right] = \sum_{p=1}^N (\lambda_p^T)^2 = (\lambda_1^T)^2 \quad (\text{D1})$$

σ_T^2 is the power of signals associated with the target :

$$\sigma_T^2 = \frac{1}{N^2} \sum_{i=1}^N \sum_{j=1}^N \left\langle |k_{ij}^T|^2 \right\rangle.$$

The trace of $\mathbf{K}^T\mathbf{K}^{T\dagger}$ can also be expressed as

$$\begin{aligned} \text{Trace} \left[\mathbf{K}^T\mathbf{K}^{T\dagger} \right] &= \sum_{i=1}^N \sum_{j=1}^N |k_{ij}^T|^2 \\ \text{Trace} \left[\mathbf{K}^T\mathbf{K}^{T\dagger} \right] &= N^2 \sigma_T^2 \end{aligned} \quad (\text{D2})$$

From Eq.D1 and Eq.D2, we deduce

$$\lambda_1^T = N\sigma_T \quad (\text{D3})$$

Now, we consider the case of the matrix \mathbf{K} . This matrix is the sum of two contributions (Eq.14) :

- \mathbf{K}^T which corresponds to the direct echo reflected by the target.
- \mathbf{K}^R which corresponds to the response of the random medium (or to additive noise).

The trace of the autocorrelation matrix $\mathbf{K}\mathbf{K}^\dagger$ is given by

$$\text{Trace} [\mathbf{K}\mathbf{K}^\dagger] = \sum_{p=1}^N \lambda_p^2 \quad (\text{D4})$$

We note σ_R^2 the mean power of signals linked with the random contribution:

$$\sigma_R^2 = \frac{1}{N^2} \sum_{i=1}^N \sum_{j=1}^N \langle |k_{ij}^R|^2 \rangle.$$

The trace of $\mathbf{K}\mathbf{K}^\dagger$ can be also expressed as

$$\begin{aligned} \text{Trace} [\mathbf{K}\mathbf{K}^\dagger] &= \sum_{i=1}^N \sum_{j=1}^N |k_{ij}|^2 \\ &= \sum_{i=1}^N \sum_{j=1}^N (k_{ij}^T + k_{ij}^R) (k_{ij}^{T*} + k_{ij}^{R*}) \\ &= \underbrace{\sum_{i=1}^N \sum_{j=1}^N |k_{ij}^T|^2}_{N^2 \sigma_T^2} + \underbrace{\sum_{i=1}^N \sum_{j=1}^N |k_{ij}^R|^2}_{N^2 \sigma_R^2} + 2 \sum_{i=1}^N \sum_{j=1}^N \Re [k_{ij}^T k_{ij}^{R*}] \end{aligned}$$

Assuming that $N\sigma_T \gg \sigma_R$ and $N\sigma_R \gg \sigma_T$ (assumptions verified *a posteriori* with Eq.18), we can neglect the third sum because $\langle \Re [k_{ij}^T k_{ij}^{R*}] \rangle = 0$ and $\text{std} \left[\sum_{i=1}^N \sum_{j=1}^N \Re [k_{ij}^T k_{ij}^{R*}] \right] = N\sigma_T\sigma_R \ll N^2\sigma_T^2, N^2\sigma_R^2$. And we finally obtain

$$\text{Trace} [\mathbf{K}\mathbf{K}^\dagger] = N^2 (\sigma_T^2 + \sigma_R^2) \quad (\text{D5})$$

From Eq.D4 and Eq.D5, we can deduce an expression for the quadratic mean of the singular values

$$\sqrt{\frac{1}{N} \sum_{p=1}^N \lambda_p^2} = \sqrt{N (\sigma_T^2 + \sigma_R^2)} \quad (\text{D6})$$

[1] G. Foschini and M. Gans, Wireless Personal Communication, vol. 6 (Kluwer Academic Publishers, Dordrecht, The Netherlands, 1998).

- [2] A. Moustakas, H. Baranger, L. Balents, A. Sengupta, and S. Simon, *Science* **287**, 287 (1999).
- [3] A. Derode, A. Tourin, J. de Rosny, M. Tanter, S. Yon, and M. Fink, *Phys. Rev. Lett.* **90**, 014301 (2003).
- [4] B. Angelsen, Ultrasound Imaging. Waves, Signals and Signal Processing. (Emantec, Trondheim, Norway, 2000).
- [5] S. Stergiopoulos, Advanced Signal Processing Handbook: Theory and Implementation for Radar, Sonar, and Medical Imaging real-time systems (CRC Press LLC, Boca Raton, FL, USA, 2001).
- [6] A. Tulino and S. Verdù, *Foundations and Trends in Communications and Information Theory* **1**, 1 (2004).
- [7] R. Sprik, A. Tourin, J. de Rosny, and M. Fink, *Phys. Rev. B* **78**, 012202 (2008).
- [8] C.-N. Nua, D. Tse, J. Kahn, and R. Valenzuela, *IEEE Trans. Inform. Theory* **48**, 637 (2002).
- [9] A. Moustakas, S. Simon, and A. Sengupta, *IEEE Trans. Inform. Theory* **49**, 2545 (2003).
- [10] I. Vellekoop and A. Mosk, *Phys. Rev. Lett.* **101**, 120601 (2008).
- [11] J. Pendry, A. M. Kinnon, and P. J. Roberts, *Proc. Roy. Soc. A* **437**, 67 (1992).
- [12] C. Prada and M. Fink, *Wave Motion* **20**, 151 (1994).
- [13] C. Prada, S. Manneville, D. Poliansky, and M. Fink, *J. Acoust. Soc. Am.* **99**, 2067 (1996).
- [14] C. Prada and J.-L. Thomas, *J. Acoust. Soc. Am.* **114**, 235 (2003).
- [15] J.-G. Minonzio, C. Prada, A. Aubry, and M. Fink, *J. Acoust. Soc. Am.* **120**, 875 (2006).
- [16] L. Borcea, G. Papanicolaou, and C. Tsogka, *Inverse Problems* **22**, 1405 (2006).
- [17] N. Mordant, C. Prada, and M. Fink, *J. Acoust. Soc. Am.* **105**, 26342642 (1999).
- [18] J. F. Lingeitch, H. C. Song, and W. A. Kuperman, *J. Acoust. Soc. Am.* **111**, 26092614 (2002).
- [19] L. Carin, H. Liu, T. Yoder, L. Couchman, B. Houston, and J. Bucaro, *J. Acoust. Soc. Am.* **115**, 259 (2004).
- [20] E. Kerbrat, C. Prada, D. Cassereau, and M. Fink, *J. Acoust. Soc. Am.* **113**, 1230 (2003).
- [21] C. Gaumond, D. Fromm, J. Lingeitch, R. Menis, G. Edelmann, D. Calvo, and E. Kim, *J. Acoust. Soc. Am.* **119**, 976 (2006).
- [22] C. Prada, J. de Rosny, D. Clorennec, J.-G. Minonzio, A. Aubry, M. Fink, L. Berniere, P. Billaud, S. Hibral, and T. Folegot, *J. Acoust. Soc. Am.* **122**, 761 (2007).
- [23] H. Tortel, G. Micolau, and M. Saillard, *J. Electromagn. Waves Appl.* **13**, 687 (1999).

- [24] G. Micolau, M. Saillard, and P. Borderies, *IEEE Trans. Geosci. Remote Sens.* **41**, 1813 (2003).
- [25] E. Iakovleva, S. Gdoura, D. Lesselier, and G. Perrusson, *IEEE Trans. Antennas Propagat.* **55**, 2598 (2007).
- [26] E. Iakovleva and D. Lesselier, *IEEE Trans. Antennas Propagat.* **56**, 825 (2008).
- [27] D. de Badereau, H. Roussel, and W. Tabbara, *J. Electromagn. Waves Applic.* **17**, 921 (2003).
- [28] H. Nguyen, H. Roussel, and W. Tabbara, *IEEE Trans. Geosci. Remote Sens.* **44**, 838 (2006).
- [29] Y. Ziadé, H. Roussel, M. Lesturgie, and W. Tabbara, *IEEE Trans. Antennas Propagat.* **56**, 1048 (2008).
- [30] T. Brody, J. Flores, J. Franch, P. Mello, A. Pandey, and S. Song, *Rev. Mod. Phys.* **53**, 385 (1981).
- [31] C. Ellegaard, T. Guhr, K. Lindemann, J. Nygard, and M. Oxborrow, *Phys. Rev. Lett.* **77**, 4918 (2003).
- [32] Y. L. Cun, I. Kanter, and S. A. Solla, *Phys. Rev. Lett.* **66**, 2396 (1991).
- [33] L. Laloux, P. Cizeau, J.-P. Bouchaud, and M. Potters, *Phys. Rev. Lett.* **83**, 1467 (1999).
- [34] A. Sengupta and P. Mitra, *Phys. Rev. E* **60**, 3389 (1999).
- [35] I. Johnstone, *Ann. Statist.* **29**, 295 (2001).
- [36] N. El-Karoui, *Ann. Statist.* **36**, 2757 (2008).
- [37] A. Aubry and A. Derode, *Phys. Rev. Lett.* **102**, 084301 (2009).
- [38] V. Marčenko and L. Pastur, *Math. USSR-Sbornik* **1**, 457 (1967).
- [39] A. Derode, V. Mamou, and A. Tourin, *Phys. Rev. E* **74**, 036606 (2006).
- [40] Y. Kuga and A. Ishimaru, *J. Opt. Soc. Am. A* **1**, 831 (1984).
- [41] E. Akkermans, P.-E. Wolf, and R. Maynard, *Phys. Rev. Lett.* **56**, 1471 (1986).
- [42] P.-E. Wolf and G. Maret, *Phys. Rev. Lett.* **55**, 2696 (1985).
- [43] A. Tourin, A. Derode, P. Roux, B. van Tiggelen, and M. Fink, *Phys. Rev. Lett.* **79**, 3637 (1997).
- [44] A. Tourin, A. Derode, A. Peyre, and M. Fink, *J. Acoust. Soc. Am.* **108**, 503 (2000).
- [45] A. Aubry and A. Derode, *Phys. Rev. E* **75**, 026602 (2007).
- [46] A. Ishimaru, Wave Propagation and Scattering in Random Media (Academic Press, New York, 1978).
- [47] V. Mamou, Ph.D. thesis, Université Paris 7 - Denis Diderot (2005, <http://tel.archives-ouvertes.fr>).

- [48] J. Goodman, Statistical Optics (Wiley & Sons, New York, 1985), chap. 5.
- [49] A. Derode and M. Fink, J. Acoust. Soc. Am. **101**, 690 (1997).
- [50] T. Nieuwenhuizen and M. van Rossum, Phys. Rev. Lett. **74**, 2674 (1995).
- [51] H. Hu, A. Strybulevych, J. Page, S. Skipetrov, and B. A. van Tiggelen., Nature Phys. **4**, 945 (2008).
- [52] D. Wiersma, M. van Albada, B. van Tiggelen, and A. Lagendijk, Phys. Rev. Lett. **74**, 4193 (1995).
- [53] M. Haney and R. Snieder, Phys. Rev. Lett. **91**, 093902 (2003).
- [54] W. Bryc, A. Dembo, and T. Jiang, Ann. Probab. **34**, 1 (2006).
- [55] D. Chambers and A. Gautesen, J. Acoust. Soc. Am. **109**, 2616 (2001).
- [56] J.-G. Minonzio, C. Prada, D. Chambers, and M. Fink, J. Acoust. Soc. Am. **117**, 789 (2005).
- [57] H. Zhao, SIAM J. Appl. Math. **64**, 725 (2004).
- [58] A. Aubry, J. de Rosny, J.-G. Minonzio, C. Prada, and M. Fink, J. Acoust. Soc. Am. **120**, 2746 (2006).
- [59] J.-L. Robert and M. Fink, J. Acoust. Soc. Am. **125**, 218 (2009).
- [60] M. Mehta, Random Matrices (Academic Press, Boston, MA, 1991).
- [61] L. Pastur, Lett. Math. Phys. **25**, 259 (1992).
- [62] C. Tracy and H. Widom, Commun. Math. Phys. **159**, 151 (1994).
- [63] C. Tracy and H. Widom, Commun. Math. Phys. **177**, 727 (1996).
- [64] K. Johansson, Commun. Math. Phys. **209**, 437 (2000).
- [65] N. El-Karoui, Acta Phys. Polon. B **36**, 2681 (2005).
- [66] M. Meckes, Electron. Commun. Probab. **12**, 315 (2007).
- [67] R. Adamczak, arXiv:math/0803.3111 (2008).
- [68] S. Chatterjee, Probab. Theory Related Fields **143**, 1 (2009).